Check for updates

Donor–acceptor complex formation by social self-sorting of polycyclic aromatic hydrocarbons and perylene bisimides†‡

Simon Soldner,[a] Olga Anhalt,[a] Menyhárt B. Sárosi, [iD][ab] Matthias Stolte[ab] and Frank Würthner [iD] *[ab]

Self-assembly *versus* complexation with polycyclic aromatic hydrocarbon (PAH) guest molecules is studied for a series of perylene bisimides (PBIs). Bulky imide substituents at the PBI guide their self-assembly into dimer aggregates with null-type exciton coupling. Host–guest titration experiments with perylene and triphenylene PAHs afford 1:1 and 1:2 complexes whose properties are studied by single crystal X-ray analysis and UV/Vis and fluorescence spectroscopy.

Electron-donor–acceptor (EDA) complexes between electron-rich and electron-poor π-scaffolds are most desirable dye aggregates as they afford light-induced charge carrier generation as required for many applications.[1–3] However, whilst the formation of EDA complexes is common for smaller π-systems such as tetracyanoethene or nitrobenzenes in combination with electron-rich polycyclic aromatic hydrocarbons (PAHs, *e.g.* tetramethyl-*p*-phenylenediamine, 1,3,5-triaminobenzenes, anthracene, carbazole) in thin films and solid state, the association constants between the two counterparts in solution remain rather modest, typically around 10 M^{-1}.[4] Unfortunately, such low binding affinities cause severe limitations for photophysical studies that typically have to be carried out in dilute solution. For the enhancement of the binding affinities for such EDA complexes, enlargement of the π-scaffolds appears as an obvious approach because by this means dispersion interactions between planar π-scaffolds should provide the desired binding strength.[5] Recent

progress in this field, albeit with binding affinities remaining still modest, was accomplished in particular for naphthalene bisimide based electron acceptors, opening up research avenues in the fields of foldamer science[6,7] and anion–π-catalysis.[8]

Among the common π-systems, perylene bisimides (PBIs) appear as a perfect choice with an expanded π-scaffold of 24 sp²-hybridized carbon and two additional nitrogen atoms. PBIs are also versatile dyes for photophysical studies due to intense absorption bands in the visible range, excellent (photo-)stability, outstanding fluorescence and reversible reduction at modest potential.[9] However, these dyes are prone to self-aggregation which is most apparent in their main industrial application as high grade colour pigments.[10] The strong cohesive forces between PBIs are also manifested in a multitude of dye aggregates, liquid-crystalline mesophases and supramolecular polymers.[11] As a consequence of the strong intermolecular interactions between PBIs, primarily by dispersion and electrostatic forces,[12] early attempts in our laboratory for preparing EDA complexes between the electron-poor π-scaffold of PBIs and electron-rich PAHs failed because of narcissistic self-sorting, *i.e.* the formation of pristine PBI aggregates that did not incorporate the electron-rich PAHs.[13] Only more recently, such complexes could be observed in solution with PBI cyclophane supramolecular hosts[14] as well as in the solid state as cocrystals.[15–18]

Here, following our recent research on larger nanographene multi-imides,[19,20] in this communication we introduce PBIs bearing bulky imide groups as supramolecular hosts for PAHs. Even for this design, our research reveals the preference of PBI for self-aggregation into dimer aggregates *via* PBI-PBI π-contacts along with weak C–H···π-interactions that are considerably stronger than those between electron-rich PAHs and PBI. Accordingly, our results showcase that EDA interactions are weak compared to the stronger non-covalent forces between electron-poor PBIs.

For our research we chose PBI receptors **3a–c** (Fig. 1a) whose synthesis was accomplished from perylene tetraester **1** and aromatic amines **2a–c** (Scheme S3, ESI‡),[21] which vary in the *para*-position of the terphenyl wedges. **3a**[21] has a bulky *tert*-butyl group while **3b** and **3c** have flexible *n*-hexyl or branched

[a] *Center for Nanosystems Chemistry (CNC), Universität Würzburg,
Theodor-Boveri-Weg, 97074 Würzburg, Germany
E-mail: wuerthner@uni-wuerzburg.de*

[b] *Institut für Organische Chemie, Universität Würzburg, Am Hubland,
97074 Würzburg, Germany*

† All UV/Vis absorption spectra of the titration studies are available in the Zenodo repository https://doi.org/10.5281/zenodo.8196841.

‡ Electronic supplementary information (ESI) available. Experimental and synthetic details, UV/Vis and fluorescence spectra, aggregation and complexation studies, crystallographic data, microscopy and theoretical calculations. CCDC 2284853–2284856. For ESI and crystallographic data in CIF or other electronic format see DOI: https://doi.org/10.1039/d3cc03704e
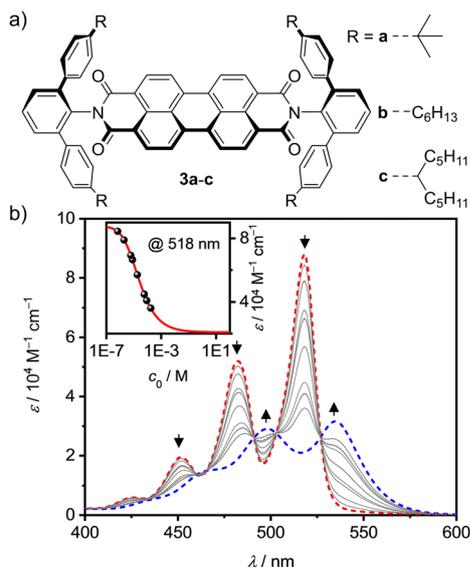
Fig. 1 (a) Chemical structures of the investigated PBIs **3a–c**. (b) Concentration-dependent UV/Vis absorption spectra (grey solid lines) for PBI **3b** in methylcyclohexane ($c_0 = 1.75 \times 10^{-4} - 1.50 \times 10^{-7}$ M) at 298 K. The dashed lines represent the calculated monomer (red) and dimer (blue) spectra according to a global fit analysis by the monomer–dimer model. The arrows indicate the spectral changes with increasing concentration. The inset depicts the monomer–dimer fit (red line) at $\lambda_{max} = 518$ nm (black symbols).
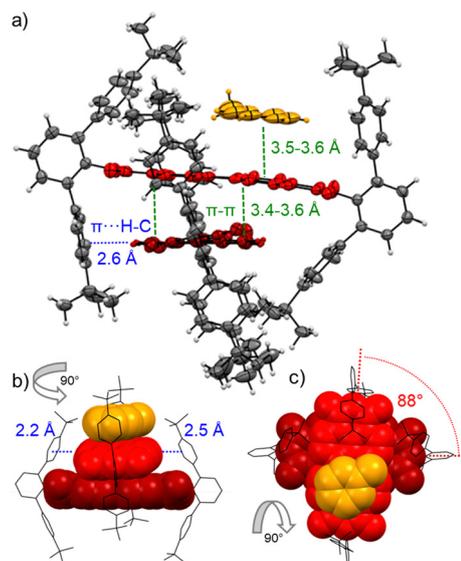
Fig. 2 Packing of PBI **3a** (red) in dimer π-stacks including a π-stacked toluene molecule (orange) in the single crystals grown from toluene and methanol in side (a and b) as well as top (c) view onto the PBIs π-system. C–H···π (blue) and π–π (green) interactions as well as the rotational displacement (red) between the PBI's N,N′-axes are indicated. Ellipsoids are set to 50% probability in (a) and the PBIs are highlighted in red. Further solvent molecules and molecular disorder are omitted for clarity.

alkyl chains, respectively. The bulky imide substituents not only endow the PBIs with excellent solubility even in low polarity solvents like methylcyclohexane (MCH) but also establish recognition sites for guest molecules like smaller PAHs. All three PBIs were characterized by high-resolution mass spectrometry (HRMS) as well as ^{1}H- and ^{13}C-NMR, UV/Vis and fluorescence spectroscopy (for details see ESI‡).

Next, we explored the effect of the bulky imide substituents on the self-assembly of these dyes in solvents of different polarity. To appreciate the effect of these substituents it is helpful to compare the studies to those previously performed for PBI dyes bearing sterically non-demanding imide substituents that enable the formation of extended dye aggregates by isodesmic self-assembly with aggregation constants (K) from about 200–600 M^{-1} in chloroform (CHCl$_3$) up to 100 000 M^{-1} in MCH for PBIs functionalized with simple alkyl or trialkyl- and trialkoxyphenyl substituents.[22] Other PBIs tailored for dimerization have K-values in a similar range of 910 M^{-1} in CDCl$_3$/MCH (1/5),[23] 2800 M^{-1} in *n*-heptane[24] and 14 100 M^{-1} in CHCl$_3$.[25] As shown by concentration-dependent UV/Vis studies, **3c** shows no aggregate growth which is explained by the steric hindrance imparted by the flexible branched alkyl chains (Fig. S3, ESI‡). However, **3b** self-assembles into discrete dimers (Fig. 1b) with an appreciably high dimerization constant of 43 000 M^{-1} in MCH.[26] The aggregation behavior was further investigated in different solvents, namely CHCl$_3$ and tetrachloroethane (TCE, Fig. S4–S7, ESI‡). In the more polar chlorinated solvents aggregation is less pronounced, *i.e.* K = 140 M^{-1} in CHCl$_3$. In comparison, **3a** shows an about sixfold stronger dimerization (K = 870 M^{-1}) than **3b** in CHCl$_3$ (Table S2, ESI‡).

This dimerization is explained by the structural features as disclosed by single crystal X-ray analyses of **3a** and **3b** (Fig. 2 and Fig. S8, S9, CCDC 2284853 and 2284854, ESI‡). Here two PBIs are closely stacked at 3.4–3.6 Å with a significant π–π-contact and an almost orthogonal rotational displacement of their respective N,N′-axes (**3a**). The spectral changes upon dimerization (Fig. 1b) are more pronounced than expected for such cross-stacked structures composed of two almost orthogonally arranged dyes where the long-range Coulomb coupling (J_{Coul}) of their molecular transition dipoles (μ_{eg} = 8.1 D) should be small.[27] However as emphasized in recent work by Spano and co-workers, low-lying charge transfer (CT) states can play a major role in PBI aggregates and should not be ignored as the resultant short-range coupling (J_{CT}) can even outperform J_{Coul}.[28] Therefore, for analyzing the PBI–PBI interactions we started with geometry optimizations of each dimer that afforded an angle between the two PBI N,N′-axes of 86° (**3a**) and 90° (**3b**) (Fig. S11, ESI‡). A negligible negative overall coupling of only −12 cm^{-1} is calculated for the perfect orthogonal case of **3b** that is, however, impressively decreased to −273 cm^{-1} for dimers of **3a** upon a minor change of the rotational offset to 86° (Table S4, ESI‡). Here, the computed J-type short-range coupling J_{CT} is considerably stronger than the H-type long-range Coulomb coupling J_{Coul}. This aggregate can accordingly be classified as a hJ dimer according to Hestand and Spano,[28] and explains the observed bathochromic shift of 610 cm^{-1} for the UV/Vis absorption spectra of the dimers compared to their monomers (Fig. 1b). For the dimers of **3b** in MCH solution as well as the dimers of **3a** in single crystals we also observe a bathochromically shifted

unstructured excimer-type emission band as well as a significant increase of the fluorescence lifetime from 4.0 ns (monomer) up to 19.9 ns (dimer, Fig. S30–S32, ESI‡).

The major interest of our study was, however, the utilization of **3a–c** as supramolecular receptors for the complexation of PAHs like perylene (P) and triphenylene (T). Here, the most obvious choice was P, whose π-surface should be more similar to the host and accordingly provide more tightly bound complexes. The binding studies were performed in the three solvents $CHCl_3$, TCE and MCH, which not only affect the PBIs self-assembly into dimers (competing equilibrium) but also the solubility of the guest molecules. Accordingly, a low host concentration was chosen for all titrations to ensure only minor presence of dimeric aggregate species (<2%).

All three PBIs **3a–c** show distinct changes in their respective UV/Vis absorption spectra with the addition of guest PAHs – however to different extend, pending their respective binding affinity due to the solvent polarity as well as the guest's solubility. A representative complexation study of **3a** with P in TCE is shown in Fig. 3 (for all other titrations, see ESI‡). The addition of guest leads to a bathochromic shift of the absorption maximum by 280 cm^{-1} to 539 nm, accompanied by an overall significant decrease of the intensity and a small increase of absorbance in the spectral range 580–700 nm. Similar results are obtained for the other hosts **3b,c** (Fig. S14–S19, ESI‡). Thus, some of the oscillator strength for the PBI S_0–S_1 transition is transferred into a low-intensity CT transition between the electron-rich P guest and the electron-poor PBI. In contrast, the titrations with T, whilst also showing a bathochromic shift, do not reveal such CT signatures (Fig. S21, S25 and S26, ESI‡). Likewise, whilst the emission for the P complex is entirely quenched, a new bathochromically shifted exciplex-type emission band is observed at 600 nm for the host–guest complex with T (Fig. S27, ESI‡).

Due to the weak binding affinity between the supramolecular receptors and the PAHs the in-depth analyses of the UV/Vis titration studies for the prevalence of 1:1 or 1:2 complexes are limited by the solubility of the guest molecules and the resultant maximal achievable degree of complexation (α_C). Only for

the highly soluble PBIs **3b** and **3c** binding constants (K_1) of up to 2262 M^{-1} for **3b** (1:1) in MCH with P at 298 K were determined. Unfortunately, here the poor solubility of P as well as the PBI's competing dimerization do not allow for a reliable analysis, whether also 1:2 complexes are formed. Similarly, NMR titration studies with the non-aggregating PBI **3c** could not discriminate between 1:1 and 1:2 complex formation, even at low temperature of 223 K in deuterated MCH (Fig. S28 and S29, ESI‡) like it was possible for PAH complexes of larger C_{64} nanographene tetraimide receptors.[19]

Still, in the more polar solvents $CHCl_3$ and TCE the higher excess of guests enabled a more accurate evaluation due the higher achievable α_C (> 60%; Fig. S12 and S23, ESI‡) whether also 1:2 complexes are formed. Studies with T in TCE show that the isosbestic points disappear after a certain amount of guest addition (Fig. 3 and Fig. S21, S22, ESI‡), which is indicative that 1:2 complexes are present in solution. Additionally, the global 1:2 fit determined with bindfit[29,30] as well as SIVVU[31] show much higher accuracy and more homogenous residual than the respective 1:1 analysis (Fig. S13/24, ESI‡). As for the dimerization, PBI **3a** shows the higher affinities for PAHs at 298 K compared to **3b** with values of $K_1 = 254$ M^{-1} and $K_2 = 23$ M^{-1} for P and $K_1 = 81$ M^{-1} and $K_2 = 13$ M^{-1} for T in TCE (for the resp. complexes of **3a,c** see Table S5, ESI‡). The observed anti-cooperativity might be explained by the imide substituents that, like a hinge, can adjust to the firstly complexed guest molecule, similarly as seen in the crystal structure of the PBI dimer shown in Fig. 2. However, opening of the hinge is possible to accommodate a second perylene guest molecule as seen in the single crystal structure of the 1:2 complex in Fig. 4a and b.

Cocrystals suitable for single crystal analysis could indeed be grown for PBI **3a** in 1:2 mixing ratio with both P and T (Fig. 4a, b and Fig. S10, CCDC 2284855 and 2284856, ESI‡) by slow diffusion of *n*-hexane (P) and methanol (T) into a 10^{-3} M solution in toluene. In the [P·**3a**·P] cocrystal each guest molecule closely stacks coplanar on top of the PBI host with a π–π distance of 3.44 Å with significant π-overlap and a rotational displacement of 71°. Additional CH···π interactions between the guest and host's imide residues with distances of 2.6 to 3.6 Å further stabilize the complex. In the [T·**3a**·T] cocrystal the situation is similar, but each guest molecule does not have the same π-distance to the PBIs π-surface (3.2–3.6 Å) and the relative orientation varies (74°, 89°). Still, short CH···π interactions (2.5–2.7 Å) support also here the complexation of the PAH guests (Fig. S10, ESI‡).

Interestingly, [P·**3a**·P] grown on quartz substrates change their colour depending on the relative orientation towards to substrate ([101],[10−1]) as well as the polarization axis of the incident light between red, deep violet and turquoise (Fig. 4c and Fig. S33–S37, ESI‡). This is due to different absorption contributions of local excitations of the PBI host, P guests as well as a prominent CT-transition, which is perpendicularly oriented to the PBIs S_0–S_1 transition. Indeed, the calculated first excited state S_1 of the cocrystal is of CT character (Fig. S38, S39, ESI‡). This transition is clearly observable in the UV/Vis spectrum in the range 600–750 nm (Fig. S38, ESI‡). While the pure host shows no absorption in this range, after addition of an excess of P an increase can be detected (Fig. 3). The higher excited states are localized either
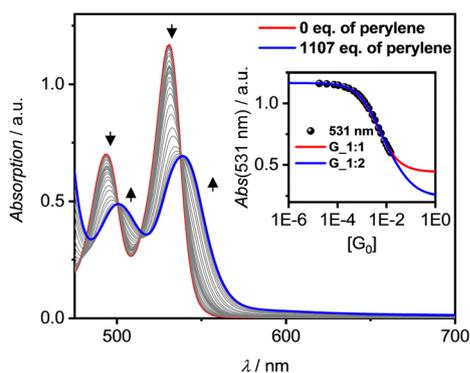
Fig. 3 UV/Vis absorption spectra (solid lines) for a solution of PBI **3a** as host ($c_0 = 1.34 \times 10^{-5}$ M, red line) and changes upon addition of P as guest (grey to blue lines, 1107 eq.) in TCE at 298 K. Resulting plot of the absorption at $\lambda_{max} = 531$ nm (black symbol) with nonlinear curve fits by the 1:1 (red line) and 1:2 (blue line) global (500–550 nm) models. Arrows depict spectral changes with increasing equivalents (eq.) of the P guest.
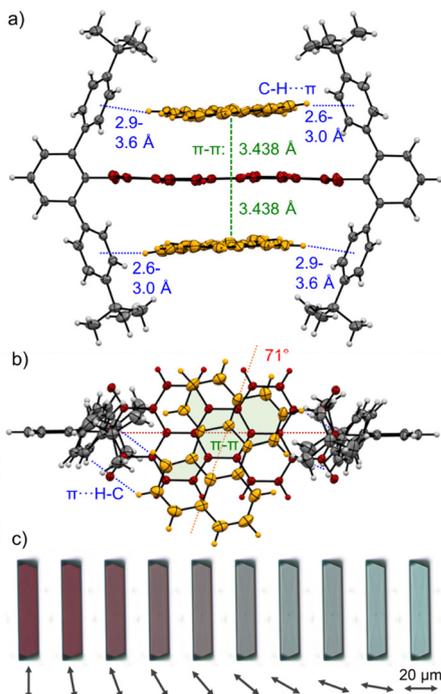
Fig. 4 Single crystals structure of the 1:2 complex of PBI **3a** (red) with two perylene guest molecules (orange) as observed by X-ray diffraction in side (a) as well as top (b) view onto the PBIs π-system. C−H⋯π (blue) and π−π (green) interactions as well as the rotational displacements (red) between the PBI *N*, *N′*-axis and the guest molecules are indicated. Ellipsoids are set to 50% probability and solvent molecules as well as molecular disorder are omitted for clarity. (c) Polarization-dependent bright-field optical microscope images of a [P·**3a**·P] cocrystal on a quartz substrate while rotating the polarization axis of the transmitted light in steps of 10° as indicated by the arrow.

on the PBI host or the P guests, in order of increasing energy. The observed experimental trend is also reproduced by theoretical calculations (Fig. S40, ESI‡): compared to the computed PBI localized excitation (LE) state of **3a** monomer, the corresponding absorptions of **3a** dimer and [P·**3a**·P] are red shifted by 455 and 1121 cm^{-1}, respectively, which is in accordance with the experimental findings. Similar calculations for the [T·**3a**·T] complex revealed no low-lying CT state between host and guest but only a LE state on the PBI unit. The stabilizing forces of [P·**3a**·P] and [T·**3a**·T] were characterized with energy decomposition analyses based on the absolutely localized molecular orbital approach (ALMO-EDA). All contributions are of similar magnitude in both complexes (Fig. S41, ESI‡). The major stabilizing interactions are provided by electrostatics and dispersion forces, while the CT contribution only plays a minor part. The lack of a significant CT contribution explains why intermolecular interactions between two electron-poor PBIs are stronger than those between an electron-poor PBI and an electron-rich P or T, thereby favouring narcissistic over social self-sorting.

In summary three sterically shielded PBIs **3a–c** were synthesized and studied as supramolecular building blocks. Concentration-dependent UV/Vis absorption studies revealed dimerization constants up to 870 M^{-1} in chlorinated solvents and 43 000 M^{-1} in MCH, as well as null-type exciton coupling

which was explained by the almost orthogonal arrangement of the PBIs in single-crystal structures. **3a–c** were next utilized for the binding of perylene and triphenylene which was comparably weak with binding constants up to $K_1 = 254$ M^{-1} and $K_2 = 23$ M^{-1} for **3a** with two perylene guests in the chlorinated solvent TCE. Single crystals provided structural evidence for the 1:2 complexes [P·**3a**·P] and [T·**3a**·T] and revealed interesting polarization-dependent absorption properties for [P·**3a**·P] that warrant further studies for such CT-cocrystals.

Conflicts of interest

The authors declare no conflict of interest.

Notes and references

1 G. Briegleb, *Elektronen-Donator-Acceptor-Komplexe*, Springer, 1st edn, 1961.
2 R. Foster, *J. Phys. Chem.*, 1980, **84**, 2135–2141.
3 D. S. Weiss and M. Abkowitz, *Chem. Rev.*, 2010, **110**, 479–526.
4 A. Das and S. Ghosh, *Angew. Chem., Int. Ed.*, 2014, **53**, 2038–2054.
5 S. Grimme, *Angew. Chem., Int. Ed.*, 2008, **47**, 3430–3434.
6 B. A. Ikkanda and B. L. Iverson, *Chem. Commun.*, 2016, **52**, 7752–7759.
7 A. Sikder, S. Chakraborty, P. Rajdev, P. Dey and S. Ghosh, *Acc. Chem. Res.*, 2021, **54**, 2670–2682.
8 Y. Zhao, Y. Cotelle, L. Liu, J. López-Andarias, A.-B. Bornhof, M. Akamatsu, N. Sakai and S. Matile, *Acc. Chem. Res.*, 2018, **51**, 2255–2263.
9 R. Dubey and F. Würthner, *Nat. Chem.*, 2023, **15**, 884.
10 M. U. Schmidt and K. Hunger, *Industrial organic color pigments*, Wiley, 4th edn, 2004.
11 F. Würthner, C. R. Saha-Möller, B. Fimmel, S. Ogi, P. Leowanawat and D. Schmidt, *Chem. Rev.*, 2016, **116**, 962–1052.
12 R. Fink, J. Seibt, V. Engel, M. Renz, M. Kaupp, S. Lochbrunner, H.-M. Zhao, J. Pfister, F. Würthner and B. Engels, *J. Am. Chem. Soc.*, 2008, **130**, 12858–12859.
13 M. M. Safont-Sempere, G. Fernández and F. Würthner, *Chem. Rev.*, 2011, **111**, 5784–5814.
14 P. Spenst and F. Würthner, *Angew. Chem., Int. Ed.*, 2015, **54**, 10165–10168.
15 M. L. Williams, I. Schlesinger, R. M. Jacobberger and M. R. Wasielewski, *J. Am. Chem. Soc.*, 2022, **144**, 18607–18618.
16 Y. Su, Y. Li, J. Liu, R. Xing and Y. Han, *Nanoscale*, 2015, **7**, 1944–1955.
17 I. Schlesinger, N. E. Powers-Riggs, J. L. Logsdon, Y. Qi, S. A. Miller, R. Tempelaar, R. M. Young and M. R. Wasielewski, *Chem. Sci.*, 2020, **11**, 9532–9541.
18 P. Yu, Y. Li, H. Zhao, L. Zhu, Y. Wang, W. Xu, Y. Zhen, X. Wang, H. Dong, D. Zhu and W. Hu, *Small*, 2021, **17**, 2006574.
19 M. Mahl, M. A. Niyas, K. Shoyama and F. Würthner, *Nat. Chem.*, 2022, **14**, 457–462.
20 M. A. Niyas, K. Shoyama and F. Würthner, *Angew. Chem., Int. Ed.*, 2023, **62**, e202302032.
21 M. Mahl, K. Shoyama, A. M. Krause, D. Schmidt and F. Würthner, *Angew. Chem., Int. Ed.*, 2020, **59**, 13401–13405.
22 Z. Chen, B. Fimmel and F. Würthner, *Org. Biomol. Chem.*, 2012, **10**, 5845–5855.
23 C. Shao, M. Grüne, M. Stolte and F. Würthner, *Chem. – Eur. J.*, 2012, **18**, 13665–13677.
24 M. M. Salfont-Sempere, P. Osswald, K. Radacki and F. Würthner, *Chem. – Eur. J.*, 2010, **16**, 7380–7384.
25 J. Gershberg, F. Fennel, T. H. Rehm, S. Lochbrunner and F. Würthner, *Chem. Sci.*, 2016, **7**, 1729–1737.
26 F. Fennel, S. Wolter, Z. Xie, P. A. Plötz, O. Kühn, F. Würthner and S. Lochbrunner, *J. Am. Chem. Soc.*, 2013, **135**, 18722–18725.
27 E. Sebastian, A. M. Philip, A. Benny and M. Hariharan, *Angew. Chem., Int. Ed.*, 2018, **57**, 15696–15701.
28 N. J. Hestand and F. Spano, *Acc. Chem. Res.*, 2017, **50**, 341–350.
29 P. Thordarson, *Chem. Soc. Rev.*, 2011, **40**, 1305–1323.
30 bindfit (Supramolecular, 2020), http://supramolecular.org/, accessed July 27th, 2023.
31 Vander Griend DA, SIVVU, https://sivvu.org/, accessed July 27th, 2023.